INSTITUTE OF PHYSICS PUBLISHING MEASUREMENT SCIENCE AND TECHNOLOGY
Meas. Sci. Technol. **13** (2002) 141–149 PII: S0957-0233(02)28686-5

A compact molecular beam line

B Riedmüller[1,2], F Giskes[1], D Glastra van Loon[1], P Lassing[3] and A W Kleyn[2]

[1] FOM-Institute for Atomic and Molecular Physics, Kruislaan 407, 1098 SJ Amsterdam, The Netherlands
[2] Leiden Institute of Chemistry, Gorlaeus Laboratories, Leiden University, Einsteinweg 55, PO Box 9502, 2300 RA Leiden, The Netherlands
[3] The National Institute for Nuclear Physics and High Energy Physics, Kruislaan 407, 1098 SJ Amsterdam, The Netherlands

Received 10 September 2001, accepted for publication 14 November 2001
Published 21 December 2001
Online at stacks.iop.org/MST/13/141

Abstract
A new supersonic molecular beam line has been attached to an existing UHV apparatus. Three different nozzles mounted on a rotatable manipulator allow for independent gas feeds. In this way, dosing sequences with different reactive gases can be carried out within a few minutes. Due to the compact design of the beam line, the apparatus does not forfeit its original flexibility and mobility. Apart from standard techniques like thermal desorption spectroscopy, low-energy electron diffraction, reflection absorption infrared spectroscopy and x-ray photoelectron/Auger electron spectroscopy, a quadrupole mass spectrometer mounted on a linear drive and viewports allows for photochemical experiments or other laser applications.

Keywords: supersonic molecular beam, time of flight calibration, rotatable nozzle manipulator, UHV, K&W technique, corrosion resistant

1. Introduction

Molecular beam techniques are widely applied to study the dynamics of molecule–surface or atom–surface interactions. These experiments contribute to the understanding of reaction mechanisms occurring on surfaces. The final aim of all these studies is to unravel the precise nature of the potential energy surface on which atoms or molecules move. Once fully understood, reaction paths and rates can be predicted. Due to the multitude and complexity of the interactions between many surface atoms and the probe molecule or atom, this problem is not solvable by one experimental approach alone. In general, the information gained from scattering molecules from surfaces is a convolution of interactions with different parts of the unit cell and the different initial states of the molecule. Quantum mechanical calculations illustrate this complexity. Presently, even supercomputers are still not sufficiently powerful to consider all physical quantities. However, these quantum calculations provide a detailed understanding of mechanistic aspects because one is able to study—in contrast to experiments—a single set of impact conditions. Note that experimentally, even if a molecule is prepared in a single state, the whole unit cell is still probed. Nevertheless, molecular beam experiments are extremely conducive because they allow one to judge the quality of theoretical models or provide starting conditions for calculations.

To probe the dynamics of surface–molecule interactions, different experimental approaches have been applied which are well documented in literature. One attempt is, for example, to study the behaviour of the backscattered molecules or atoms. Angular distribution, energy transfer or rotational or vibrational state distributions give indirect information on the interaction potential [1–5].

An extension of these techniques is to investigate the interaction of molecules prepared in specific quantum states. This has been successfully accomplished for the two diatomics NO [6–9] and H_2 [10]. By means of an electrostatic hexapole, NO molecules can be oriented and one can study the reactivity of the N and O ends of the molecule independently [6, 7]. Further progress has been accomplished recently by McCabe *et al* [11], which succeeded in the first eigenstate-resolved gas–surface studies of methane [12, 13].

Molecular beam techniques have also been used to study the thermodynamics of adsorption. By combining a molecular beam with a single-crystal adsorption microcalorimeter, Borroni-Bird and King [14] developed a technique to measure the heat of adsorption of molecules as a function of coverage.

Very often, molecular beams are also used as a 'clean' method to prepare overlayers in a very well-defined way. This is particularly advantageous when dealing with vacuum pollutive gases such as, e.g., water. By means of molecular beams, the molecules impinge exclusively on the sample. This results in an instantaneous recovery of the base pressure even after long exposures. In addition, when following gas–surface reactions, one can be certain that the products are formed by the sample and do not appear due to side reactions induced by, for example, hot filaments or other active metals of the UHV apparatus.

Furthermore, by means of molecular beams adsorption states can be prepared which are inaccessible by thermal energy because of, for example, an activation barrier to adsorption. These states and their corresponding activation barriers are of particular interest, because of their relevance to heterogeneous catalysis. The knowledge of surface intermediates and their chemistry is the key to the understanding of reaction mechanisms. For this purpose, several apparatus have been designed over the past decades to combine molecular beams with standard surface techniques such as thermal desorption spectroscopy (TDS) [15–20], Auger electron spectroscopy (AES) [15–17], reflection absorption infrared spectroscopy (RAIRS) [20], low-energy electron diffraction (LEED) [15–19], scanning tunnelling microscopy (STM) [21] and/or electron energy loss spectroscopy (EELS) [15].

The ultimate aim of catalytic research is to understand the elementary steps of a reaction. The knowledge of the gas–surface interaction covers an important part of the catalytic process, namely adsorption and/or dissociation. However, adsorbed surface species have to react with each other before the desired product is formed. Following these surface processes in time can only be established by ultrafast pulsed lasers because these reactions usually occur in the femtosecond regime [22]. This technique is unique because one can follow the evolution of a product or the disappearance of a reactant during the reaction.

To be fully capable to study both processes, a molecular beam apparatus is required which provides both techniques and is able to operate in a laser laboratory. We therefore designed a compact molecular beam line and attached it to an existing UHV apparatus that was originally constructed to study the interaction of surface adsorbates with light [23]. To retain optimal flexibility for the future our most important requirement was to be able to operate the beam line with a combination of reactive and/or corrosive gases. Especially, fast dosing sequences with different gases should be possible with a minimum time delay between different exposures.

2. Design criteria

In order to attach a molecular beam line to an existing UHV chamber [23], the following design criteria were formulated:

(1) Resistance against corrosive and/or aggressive gases, especially if they are used consecutively. Emphasis was put on gases like NO, O_2, H_2O vapour and HCl.
(2) A flux in the order of 1 Ml s^{-1} should be achieved.
(3) The design should allow for dosing sequences with different gases and/or gas mixtures with the least possible time delay ($\Delta t \approx 2$–5 min).
(4) The translational energy of the beam should be variable and exhibit a narrow distribution, which should be experimentally measurable.
(5) The design should allow for the implementation of the technique developed by King and Wells (K&W [24, 25]) to measure sticking probabilities of molecules or atoms to be implemented.
(6) The molecular beam line has to fit on the existing frame of the experiment and should not substantially increase the compact size of the original experiment to retain the transportability.
(7) The new beam line should not interfere with other experimental techniques like XPS/AES, RAIRS and LEED.
(8) All major interior components of the molecular beam line should be accessible without breaking the vacuum of the main chamber.

3. Implementation and performance

3.1. Molecular beam line

Our first requirement was resistance against various aggressive gases, especially if they are used consecutively. Corrosion problems are mainly expected where high gas pressures predominate. This is mainly the case in gas lines and the expansion chamber. Special care had to be taken to protect experimental equipment such as pumps and pressure gauges because their lifetimes might be severely shortened if they are operated under aggressive conditions. In contrast, corrosive damage is negligible in the HV and UHV sections of the set-up since the partial pressures of the aggressive gases are extremely low. In this sense, to meet corrosion resistance we mainly focused on the gas inlet system, expansion chamber, pressure gauges and pumps. As aggressive or corrosive gases are pollutive and a hazard to human health, we put major effort on minimizing its overall consumption by choosing a compact design with a very short nozzle to surface distance. In the following corrosion resistance will only be discussed in case of relevance.

Figure 1 shows a 3D illustration of the molecular beam line and its facilities where the main UHV vessel and the sample manipulator are depicted schematically. The main vacuum chamber is a cylinder which is horizontally mounted onto a frame. For simplicity, surface-sensitive techniques such as RAIRS, XPS or LEED are not depicted. They are located at the prolongation of the cylindrical chamber. The sample manipulator is represented schematically by a rod, situated in a bellow, which is mounted on an XY-stage.

Because of the geometry of the existing experiment, the molecular beam has to cross the vacuum chamber perpendicular to the translational motion of the sample, with the mass spectrometer on the opposite site. To meet chemical resistance for the chemicals specified above, all metal parts are made of corrosion-resistant steel (SS316).

The requirement of a short distance between sample and nozzle in combination with three differentially pumped stages demands that the beam line is incorporated into the main vacuum system. A prefabricated part of the beam line consisting of two stages had to be implemented into the main

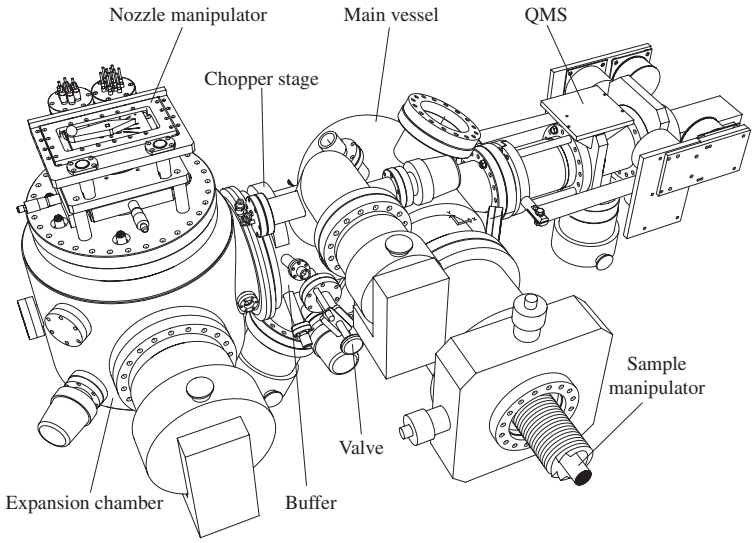

Figure 1. A 3D illustration of molecular beam line, main vessel and QMS facility. The main vessel and sample manipulator are only drawn schematically.

vacuum system. Those two stages, referred to as the buffer and chopper stages, are separated by a mini-valve with a slide mechanism. The buffer stage represents a pure pumping stage, the sole aim of which is to suppress the effusive component of the beam. A connection to the main chamber is made via a small circular aperture. The chopper stage contains a beam shutter, chopper wheel and related electronics. The molecular beam originates from a free-jet expansion through a small orifice into the vacuum. This takes place in the expansion chamber which is equipped with a multi-functional nozzle manipulator. Expansion and chopper chambers are connected by a flange which allows for easy access to all interior facilities of the beam line. With the mini-valve shut, repair and/or servicing of all crucial components can be conducted without breaking the vacuum of the main chamber. In line of sight with the molecular beam, a differentially pumped quadrupole mass spectrometer (QMS) is mounted on a linear drive. The precise description of the QMS setup is given in the following section.

The expansion chamber is pumped by a corrosion-resistant Pfeiffer TMU 520-C turbo-drag pump in combination with an Alcatel rotary vane pump (type 2063C2). Both pumps require special lubricant (Fomblin type) to properly operate under aggressive chemical conditions. Due to the high gas load into the expansion chamber, a combination of high capacity pumps has to be chosen to achieve a large flow rate through the nozzle without exceeding the critical pressure above which either the molecular beam or the pump collapses. Furthermore, optimum geometry has to be chosen to exploit the full capacity of the pumps. Therefore, the turbo-drag pump with a constant capacity of 520 l s^{-1} (for N_2) at pressure below 5×10^{-3} mbar is mounted directly, horizontally to the expansion vessel. The pump operates reliably at a maximum pressure of 5×10^{-3} mbar for hours. As a consequence of these inconvenient operating conditions, efficient water cooling is essential due to heat evolution. The capacity of the rotary vane pump (35 m^3 h^{-1}) was chosen such that the maximum force pressure (10 mbar) of the turbo drag pump is two orders of magnitude lower than the maximum pressure specified by the supplier. This is to minimize the power consumption and to extend the lifetimes of pump and supply. The chopper stage is pumped by a similar combination of pumps. Low pressure is achieved by a chemically resistant Pfeiffer TMU 260C turbo-drag pump with a capacity of 190 l s^{-1} backed by an additional rotary vane pump (Alcatel 2015C2, 15 m^3 h^{-1}). For the sake of a short nozzle to surface distance, the pump could not be directly attached to the chopper stage. A 90° elbow had to be introduced to meet spatial requirements, which results in a less favourable geometry in terms of pumping efficiency. Nevertheless, with maximum gas load, the pressure does not rise above 1×10^{-5} mbar. The resulting effusive beam can be easily absorbed by the buffer chamber, which is pumped by a Pfeiffer TPU 180H turbo-drag pump (180 l s^{-1}). Due to the low volume flow rate into this stage, the turbo-drag pump is attached to the fore-vacuum of the main chamber [23]. Under operational conditions, the pressure rises to 1×10^{-7} mbar at maximum. This is low enough to perform accurate K&W measurements without difficult corrections, because the contribution of the effusive component to the total pressure rise in the main chamber amounts to less than 1%.

The upper part of figure 2 shows a 2D top view of the beam line, main vacuum chamber and QMS assembly. The solid line (labelled with A) indicates the position of the molecular beam. In the middle panel of figure 2, a cross-section cut vertically through the beam path is plotted to illustrate interior components. A viewport, mounted perpendicularly to the molecular beam direction, provides a clear view of the sample surface. This facilitates sample and skimmer alignment and has the advantage that chopper and beam shutter performance can be checked by eye.

Working with aggressive gases demands certain safety precautions not only for man and environment, but also for the equipment. Even though all components are specified to be chemically resistant, there are always certain upper concentration limits which should not be exceeded. Therefore, simultaneous pressure monitoring of all stages is essential, in combination with a well-controlled gas inlet system. The

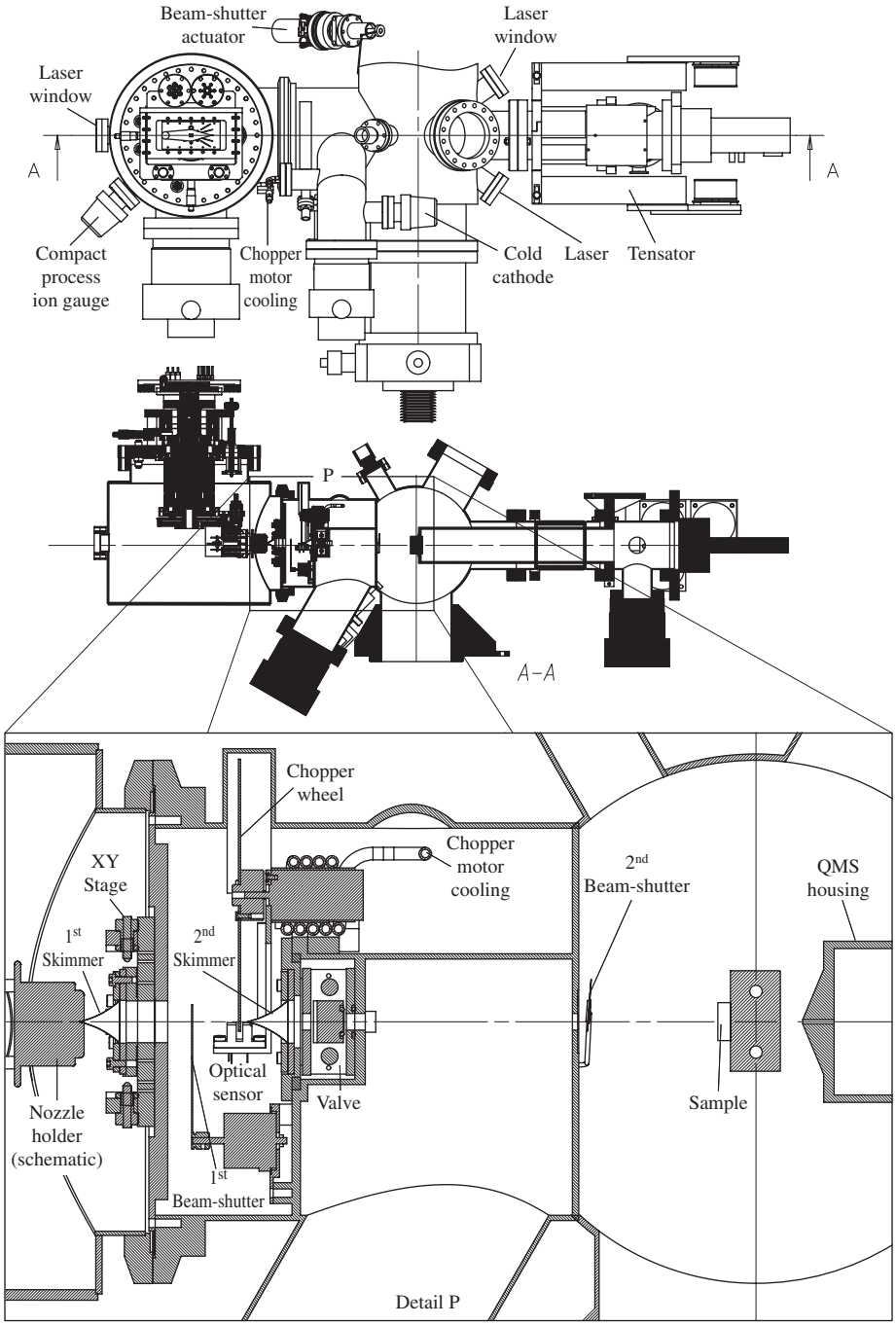

Figure 2. The upper part shows a top view of the molecular beam, the middle part a cross section of the side view. The cut has been made along line A. In the lower part a zoom-in of the side view is depicted. All crucial internal components of the beam line are magnified.

large pressure gradient over the operating beam line demands different pressure gauges for the stages. Due to the high pressure in the expansion chamber, a Pfeiffer compact process ion gauge suited for operation under aggressive conditions, with a pressure range of 10^{-6}–1000 mbar, is mounted on the expansion stage (see figure 2). This enables one to keep track of the pressure even during an accidental pressure irruption. The pressures of buffer and chopper stages are measured by Pfeiffer cold cathode gauges. Decisive for this choice was the lower pressure limit of 5×10^{-11} mbar which allows one to accurately judge the quality of the vacuum in the beam line with respect to the main chamber when the beam is not operated. All gauges can be controlled by a single unit. For every channel of the controller, pressure thresholds can be set, which are linked to a relay output. These outputs actuate electro-pneumatic valves placed between the gas mixing cabinet and nozzles, which safeguard the maximum gas load in the individual stages.

In the lower part of figure 2, a section of the molecular beam design containing crucial components is magnified. On the left-hand side, one of the nozzles situated in a radiation shield housing is depicted schematically. Expansion and chopper chambers are separated by a stainless steel plate bolted

to the flange connecting the chopper chamber. The metal-to-metal connection serves as a seal. On top of this plate, an XY-stage is mounted which carries the first skimmer (Beam dynamics, model 1, $\varnothing = 0.5$ mm) which is made of Ni. With two opposing micrometer-screws, the position of the skimmer can be aligned accurately with respect to the beam path. Presently, it is not possible to move the skimmer under vacuum but the design is such that skimmer manipulation from outside can be implemented quite easily. However, it turned out that due to the rigid construction the precision of the alignment was not affected by vacuum forces which rendered any efforts in this regard unnecessary. The second skimmer ($\varnothing = 1.3$ mm) is clamped between two metal rings which are bolted to the front of the mini-valve. This, together with the aperture connecting to the main chamber, determines the axis of the beam line. The positions of skimmers and nozzle determine the size of the beam spot dependent on the nozzle sample–surface distance. If the sample surface is aligned with respect to the axis of the main chamber, the nozzle to sample surface yields a distance of 330.5 mm. With these default values, a circular spot of 6 mm in diameter can be projected onto the sample surface (typically 10 mm in diameter) and allows a maximum angle between beam axis and sample normal of 55° with the total beam-flux still on the sample surface.

The molecular beam can be blocked by a beam shutter made of stainless steel which is actuated by a commercially available rotary solenoid. To achieve chemical resistance and to reduce degassing, minor modifications were necessary. The copper wire was substituted by one with a polyimid coating which is highly inert and does not contain unwanted plasticizer. For the body of the coil, the properties of Kapton suited the purpose. The solenoid can be switched by an external dc voltage which allows one to block or unblock the beam within less than 1 ms. Small gas pulses are provided by chopping the beam with a spinning aluminium wheel containing two slits placed opposite to each other. A large diameter was chosen to attain stable vibration-free revolutions. Therefore, the elbow-shaped chopper-chamber had to be equipped with a convexity to fit the size of the wheel. Losses in time resolution due to the finite initial pulse duration are suppressed by a 0.5% duty cycle. With a typical chopper frequency of 250 Hz, a pulse duration of 10 μs can be achieved. The copper wheel is driven by a three-phase brushless dc servomotor purchased from Minimotor SA. To prevent overheating, the motor is wedged into a copper pipe surrounded by copper tubings, which is connected to a coiling water circuit (see also the upper part of figure 2). The trigger for the instrument of the TOF measurement is supplied by a transmissive optical sensor (TCSS1100/2100) mounted at a 10° angle with respect to the beam axis. The internal Schmitt trigger of the component leads to an acceptable rise time of 50 ns, which is much faster than the time resolution of the TOF measurement.

A small additional compartment behind the second skimmer contains the mini-valve. The internal vacuum seal is made by pressing a metal plate onto a Teflon-based O-ring. Metal springs provide the necessary sealing pressure enforced by the ambient pressure when the chopper stage is pressurized. The valve can be opened and shut by a push/pull actuator with a position lock.

The second beam shutter, located in the main chamber, consists of an inert, transparent mica plate clamped on a steel holder connected to a metal cantilever arm, which can be actuated from outside the vacuum by a rotary drive (see also the upper part of figure 2). The motion of the beam shutter is automated by a rotary solenoid attached to the rotary drive. Short opening and closing times are achieved by applying a pulsed electrical current.

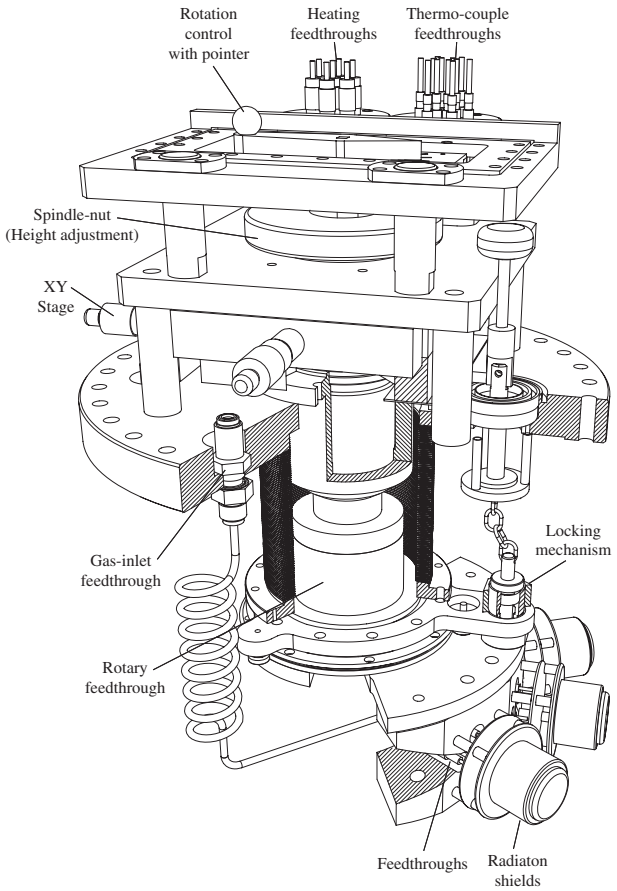

Figure 3. Drawing of the nozzle manipulator. Nozzles and nozzle-heating facilities are hidden under the radiation shields.

The nozzle manipulator represents the heart of the new beam line (figure 3). It unifies three individually functioning nozzle assemblies, equipped with heating facilities and separate gas supplies. A massive stainless steel block, mounted on a rotary drive, serves as a carrier for the three nozzle assemblies. A rotary drive is situated in a bellow which is mounted into a wide bore XY-translation stage. Two cross roller-bearing slides on top of the XY-stage are mounted to compensate for torque forces induced by the long bellow. The Z-motion can be manipulated by a spindle nut. A travel range of 25 mm for all motions is sufficient to position the nozzle in front of the skimmer with high precision. Individual settings for different nozzles can be reproduced reliably.

The rotational movement is restricted to five fixed positions by a locking mechanism. A pointer on top of the manipulator indicates which nozzle is in front of the skimmer. The bisecting lines of the angles between two nozzle assemblies define two special positions with a clear view of the sample along the beam axis through bores drilled into the steel block (see also figure 4).

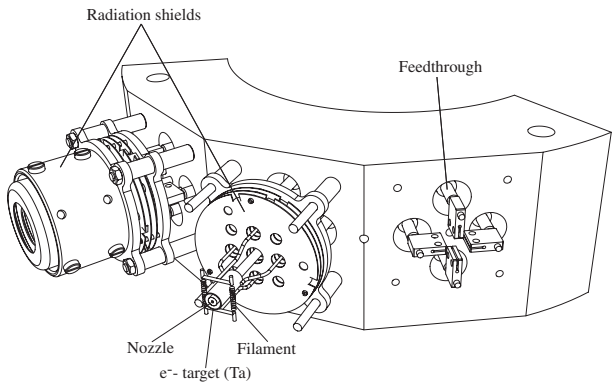

Figure 4. Drawing of the nozzle holder. The left nozzle-assembly is complete. From the middle nozzle, the radiation shields are taken off to illustrate heating devices. The right assembly shows the copper supports for the filaments and the electron beam target.

A centre-pin, kept in position by a metal spring, locks the rotational motion. To rotate the manipulator, the centre-pin, connected by a chain to a push/pull drive has to be retracted. The fragile skimmer is protected against mechanical damage which might occur during rotation. To prevent the push/pull drive being actuated while the X-drive is not in its maximum outer position, an aluminium plate is mounted on the bottom of the XY-stage.

Spatial limitations on the steel block constrict the design of the nozzle assembly. Heating filaments, thermocouples, electrical connections, gas feed and radiation shields have to be realized within a few cubic centimetres. As determined by the geometry, electrical connections and gas lines have to be made from the backside of the steel block. Consequently, a straight in-line nozzle was chosen to meet these spatial requirements. Nozzles consist of a W tips joined to Mo tubes. A gas-leak-tight junction is realized by e^--beam welding. The tips made from a tungsten rod are hollowed out from one side by spark erosion. For the different nozzles, orifice diameters between 50 and 80 μm are chosen and fabricated by a commercial workshop. The Mo tubes have been brazed into a stainless steel cup connected to the gas line which also serves as a nozzle holder. This holder is bolted to the back of the stainless-steel block (see figure 4) in such a way that the nozzle extends to the opposite side through a bore. Four feedthroughs centred around the nozzle serve as mounts for filaments and electron bombardment targets. Nozzles are heated indirectly by thermal radiation from a hot tantalum tube which is bombarded by electrons provided by two thoriated-tungsten filaments placed perpendicular to the tube. Small cups of thin tantalum foils surround all hot parts and serve as radiation shields. C-type thermocouples, spot-welded on each tip of the nozzles, form the basis for electronic temperature control. Under maximum gas load, nozzle temperatures up to 2000 K can be easily achieved by a filament current of 9 A and a bias voltage of 600 V on the Ta tube.

In most molecular beams studies, seeding techniques are used to vary the translational energy of the beam. This requires mixing of different gases with well-defined ratios. By chemically resistant mass-flow controllers (Bronkhorst F-201C-FA-11-Z), located in a separate gas cabinet, total volume-flow rates and mixing ratios can be adjusted, which guarantees reproducible beam energies and fluxes. Stagnation pressures behind nozzles are monitored by single-ended pressure transducers (MKS-700 series). A 15 μm particle filter placed on the gas-line vacuum connector protects the nozzles from clogging. The gas feed can be interrupted by three electro-pneumatic valves, placed outside vacuum and close to the nozzles. Additional manual toggle valves connecting gas lines and a rotary vane pump form individual bypasses for each nozzle. A bypass is used to pump the remaining gas behind the nozzle after the gas feed has been stopped. Afterwards, a different nozzle can be operated. Typically within a few minutes, the new beam has stabilized and the experiment can proceed. This is fast enough to expose the sample to different gas mixtures in a controlled and reproducible manner and fulfils requirement (3) satisfyingly.

Let us focus on the beam performance. A crucial quality feature of a molecular beam line is the maximum achievable flux. With the current setup, the flux cannot be directly measured but it can be estimated. This quality check was carried out using a beam consisting of 2% O_2 seeded in He with O_2 as a test gas. The number of molecules can be computed assuming ideal gas behaviour. The flux is given by

$$\frac{\mathrm{d}n}{\mathrm{d}t} \approx \frac{\Delta p S}{k_\mathrm{B} T} \tag{1}$$

with S the pumping speed for oxygen, T the temperature of the system, k_B Boltzmann's constant and Δp the pressure rise induced by oxygen. The partial oxygen pressure can be determined by calibrating the QMS reading against the ionization gauge of the main chamber, which has to be corrected for the O_2 ionization probability (supplied by the manufacturer). For the pumping speed S, we took 450 l s^{-1} as specified by the supplier of the TMP of the main chamber. The corrected oxygen-induced pressure rise yielded 7×10^{-9} mbar. This results in a flux of approximately 0.18 Ml s^{-1}, which is acceptable with respect to the chosen seeding ratio.

3.2. Beam detection and TOF techniques

In the line-of-sight of the molecular beam, a QMS mounted on a linear drive serves as a time of flight detector. Note that this could only be realized by removing the sample exchange mechanism of the old design [23]. Consequently, sample exchange without breaking the vacuum is no longer possible.

The mass spectrometer was specially manufactured for our purposes. Its design is based on the Balzers QMA400 model but possesses, instead of a 90° off-axis detector, an inline arrangement for detection. Molecules or atoms are ionized by a cross-beam ionizer. The mass filter consisting of 200 mm long Mo rods and 8 mm in diameter, combined with a 2.25 MHz radio-frequency generator, allows for a mass range up to 511 amu. Ion optics, emission and extraction voltages are computer controlled. Thereby, optimum settings for TOF measurements can be found easily. A channeltron (Burle-type 4870V) provides sharp pulses with a typical duration of 5 ns which allows for single ion counting. The pulses are amplified and height selected by a home-built pulse shape amplifier and fed to a multi-channel scaler (MCS), purchased from EG&G (Turbo MCS). The quadrupole mass analyser is situated in a stainless steel housing, which is differentially

pumped by a Pfeiffer turbo-drag pump (TPU062H, 56 l s^{-1}). To improve pumping speed and reduce back diffusion of especially hydrogen into the QMS-housing vacuum, the turbo-drag pump is connected in series with a second pump of the same type which is backed by a Balzers MD4TC diaphragm pump. A stainless steel cup with a small orifice ($\varnothing = 3.5$ mm), bolted to the QMS housing, shields the cross-beam ionizer from molecules/atoms which do not impinge into the ionization volume along the beam axis. The upper and the middle parts of figure 2 show the top and side views of the QMS assembly, which is suspended from the main frame via a YZ-stage (not depicted). Thereby, the QMS can be aligned with respect to the beam axis. A bellow provides the necessary flexibility and a translation range of 200 mm. To move the QMS along the beam axis, a linear drive is mounted to the YZ-stage which supports the QMS assembly and the bellow connecting to the main chamber. The linear motion is driven by a worm shaft mechanism and guided by cross-roller bearing slides. By this means, reproducible positioning of the QMS with high precision is guaranteed. TOF measurements can be conducted with a variable flight path ranging from 266 to 466 mm. Note that the flight path is determined by the distance between the chopper wheel and QMS ionizer. For laser desorption or photodissociation experiments two quartz viewports are mounted to the left and right-hand sides of the QMS assembly. Under specular conditions, laser light impinges at an angle of 37.5° with respect to the surface normal. Desorbing molecules can be detected at any angle by rotating the crystal. The orifice of the differentially pumped QMS housing allows for angular resolutions between 1° and 4° dependent on the flight length. For time-resolved measurements, the length of the flight path can be adjusted between 55 and 200 mm, where the limits are determined by the size of the QMS housing and the translation range of the linear drive. Note that the transfer width of the QMS assembly is sufficiently long to perform sensitive TDS measurements with a sample to QMS distance of a few millimetres.

3.3. TOF calibration and beam energies

To determine the mean energy of a molecular beam expanded from a CW nozzle, the beam has to be chopped into pulses by a chopper wheel with a short duty cycle. Creating short pulses is advantageous because measured TOF distributions are convoluted with the chopper slit function. Clearly, if long duty cycles are applied, the chopper function dominates the TOF spectrum and only the rising and falling edge of the measured gas pulse contains the shape of the TOF distribution. To measure the shape of the TOF distribution accurately and to facilitate the fitting procedure the broadening of the TOF distribution induced by the chopper can be reduced by small slits and by operating the chopper at high speeds. In our case, the beam is therefore modulated by a chopper with a 0.5% duty cycle at 500 Hz. The mechanical modulation of the beam in combination with the QMS-detection method causes some calibration problems because the point of time at which the beam passes the chopper slit is unknown on the measured timescale. This is caused by the fact that the trigger pulse generated by the optical sensor does not coincide with the pulse of molecules/atoms produced by the chopper wheel. In addition, the detection method of the molecules or atoms by a QMS adds an additional offset to the total flight time because the ionizer and not the multiplier of the QMS represents the arrival point of the flight distance of the neutral species. The total mean flight time t_{total} is therefore composed of the following contributions:

$$t_{\text{total}} = t_{\text{TOF}} + \Delta t_{\text{trig}} + \Delta t_{\text{elec}} + \Delta t_{\text{QMS}} \tag{2}$$

where t_{TOF} is the mean flight time; this is the sought value from which one can compute the mean translational energy. Δt_{trig} and Δt_{QMS} are offsets caused by the way of triggering (Δt_{trig}) and the time delay in the QMS (Δt_{QMS}). For the sake of accuracy, we assume an additional offset Δt_{elec} which might be caused by electronic delays of the optical sensor or the MCS. Since the QMS detector can be moved along the beam axis, the flight distance s from chopper to detector can be varied from 266 to 466 mm. Therefore, t_{total} can be measured as a function of s. By linear extrapolation of t_{total} to $s = 0$ mm, the sum of all time delays $\Delta t_{\text{trig}} + \Delta t_{\text{elec}} + \Delta t_{\text{QMS}}$ can be derived. This method has been applied to an oxygen beam (2% O_2/He) for various chopper frequencies. The results are depicted in figure 5 (left panel). Different chopper speeds are given in terms of the time between two consecutive slit passages $\frac{1}{2}\tau_{\text{chopper}}$. Clearly, all lines have to be parallel because the slopes of the linear fits are equivalent to the reciprocal value of the mean speed. Note that knowing the total delay is already sufficient to fit TOF spectra. However, it is important to determine all contributions separately, especially their dependencies on chopper frequency, molecular/atomic mass and QMS settings, to be able to judge the quality and reproducibility of the measurement. Furthermore, the knowledge of Δt_{QMS} is important for calibrating the absolute time axis of photodissociation experiments.

As is evident from the plot (figure 5 (left panel)) the direction of rotation of the chopper with respect to the position of the optical sensor is such that the trigger event precedes the intersection of the chopper slit with the molecular beam. This is because the total mean flight time increases with decreasing chopper speed. The time delays at $s = 0$ mm for the different chopper periods can be plotted as a function of $\frac{1}{2}\tau_{\text{chopper}}$ (see figure 5 right panel). As the trigger delay is proportional to the trigger period, the intercept of a linear fit yields the sum of the flight time through the QMS for oxygen and the electronic delay. The slope yields the trigger delay divided by the chopper period. Consequently, the contribution of Δt_{trig} can be separated from $\Delta t_{\text{QMS}} + \Delta t_{\text{elec}}$. If this procedure is repeated for molecules/atoms with large differences in molecular/atomic mass, one can distinguish between Δt_{QMS} and Δt_{elec} because the flight time through the QMS is m/e-dependent. In an ideal in-line QMS, ionized molecules or atoms are extracted from the ionizer volume by a dc voltage. This acceleration results in a constant ion velocity. After having passed the mass filter the ion hits the detector, resulting in a current pulse which is electronically modified and fed to the MCS board. Neglecting all accelerating and decelerating effects induced by the ion optics of the QMS, it can be easily shown that Δt_{QMS} is proportional to the square root of the mass-to-charge ratio ($(m/e)^{\frac{1}{2}}$). To determine the flight time through the QMS, time delays for singly and doubly charged ions of Xe, Ar, O_2, He and CH_4 have been measured. Results are depicted in figure 6 (left

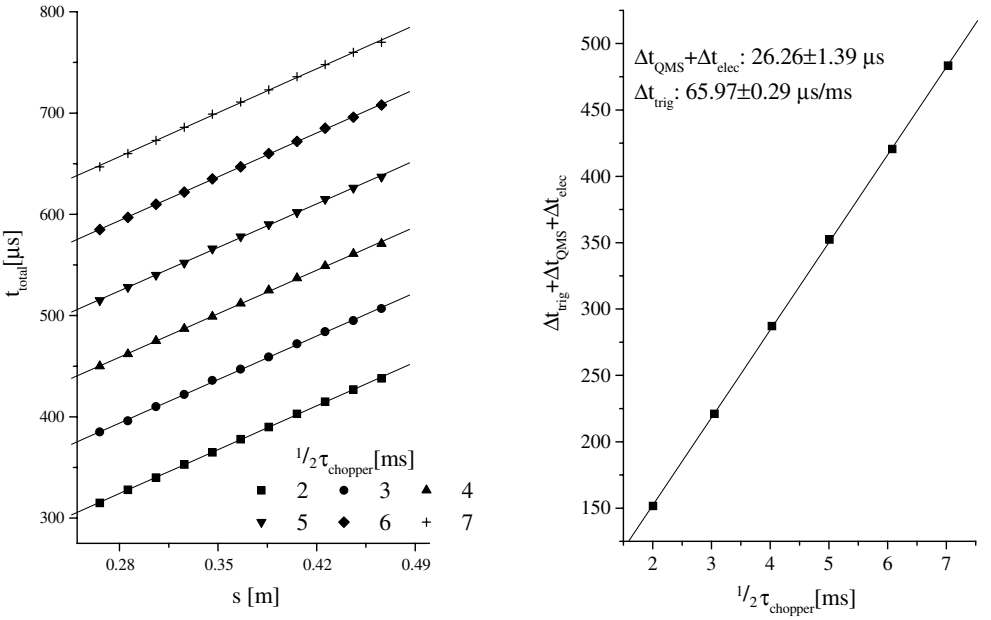

Figure 5. Left panel: the total mean flight time of an O_2 beam seeded in He, plotted as a function of the chopper–QMS distance s. Data have been taken at various chopper frequencies. $\frac{1}{2}\tau_{\text{chopper}}$ denotes the time difference between two consecutive slit passages. Solid lines are linear fits through the data points. The intercepts with the y-axis yield the sums of trigger, QMS and electronic time delay denoted as Δt_{trig}, Δt_{QMS} and Δt_{elec}, respectively. Right panel: sum of time delays plotted as a function of $\frac{1}{2}\tau_{\text{chopper}}$. The solid line is a linear fit through the data points. The intercept with the y-axis denotes the sum of Δt_{elec} and Δt_{QMS}; the slope multiplied by $\frac{1}{2}\tau_{\text{chopper}}$ equals the trigger time delay Δt_{trig}.

panel). A linear fit through the data points yields a value for the intercept equivalent to Δt_{elec} of approximately 1.05 ± 0.91 μs. Note that the scatter in the data points is not due to statistical noise: the error bars on the data points are smaller than the size of the data points. The deviation from the linear behaviour is a consequence of the *ad hoc* assumption that the QMS acts as a linear accelerator. The scatter and especially the linearity of the data strongly depend on the settings of the ion optics. In our study, optimum settings have been chosen to minimize Δt_{QMS} while retaining mass resolution and high transmission.

With the time delays determined, one can now fit the TOF distribution to a shifted Maxwell–Boltzmann distribution convoluted over the finite slit width [26] of the chopper. An example of an TOF measurement performed with an O_2 beam (2% O_2 in He, $T_n = 300$ K) is given in figure 6 (right panel). Raw data are represented as a solid line. The corresponding fit, indicated as a dotted line, yields a mean energy of 0.43 eV with an energy dispersion of $\langle \Delta E \rangle / E \approx 16\%$. This is sufficiently low to conduct energy-resolved measurements. The deviation between fit and data at the high t_{TOF} edge of the distribution is most probably due to trapping of molecules in the ionizer of the QMS which causes a pump tail.

To judge the quality and accuracy of the TOF setup, the experimental value of the mean energy can be compared to the theoretical value which can be computed assuming ideal behaviour. The theoretical energy E_{theo} is given by [27]

$$E_{\text{theo}} = \frac{5}{2}\left(\frac{m_{O_2}}{X_{O_2} m_{O_2} + X_{He} m_{He}}\right) k_B T_n \qquad (3)$$

where T_n is the nozzle temperature, k_B is the Boltzmann constant, X is the mole fraction and m is the molecular/atomic mass. The computation yields a value for E_{theo} of 0.45 eV, which is about 4.6% higher than the measured one. To illustrate the origin of this deviation, it is instructive to focus on the velocities instead of the energies. In the ideal case, He atoms and O_2 molecules travel with an identical mean velocity v_{theo} of 1653 m s^{-1}. This value compares well to the He velocity ($v_{He} = 1650$ m s^{-1}) determined experimentally for the same beam. However, O_2 molecules are slightly slower ($\Delta v = -29$ m s^{-1}) than the He atoms. This effect is also known as the velocity slip, which is due to non-ideal behaviour of the expansion mixture [27], and accounts for the energy reduction of 4.6%. In essence, the results indicate that the calibration procedure yields the correct mean energies.

4. Conclusion and summary

In summary, we have designed a compact corrosion-resistant supersonic molecular beam line, which has been attached to an existing UHV apparatus. Supersonic molecular beams are created by gas expansion from one of three independently operating nozzles. This allows us to perform dosing sequences with different reactive gases within short time intervals. Due to the compact size of the molecular beam line, the size of the setup could remain limited so that the flexibility and mobility of the existing setup could be retained. A movable QMS provides sensitive TDS measurements and determination of the beam energy. Two viewports provide the necessary optical access for laser light, enabling future photochemical and/or other laser experiments.

Acknowledgment

The authors would like to thank Mischa Bonn for carefully reading the manuscript. This work is part of the research programme of the 'Stichting voor Fundamenteel Onderzoek

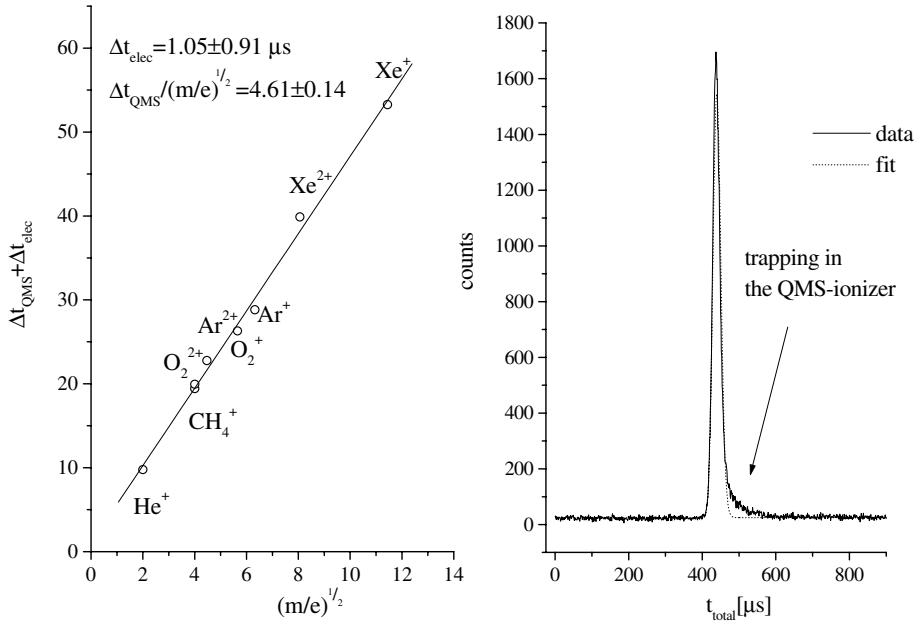

Figure 6. Left panel: sum of electronic and QMS time delay are plotted against $(m/e)^{\frac{1}{2}}$ for various ions. A linear fit yields the electronic time delays Δt_{elec} and the flight time through the QMS. Right panel: time of flight distribution of an O_2 beam seeded in He (solid line). The x-axis denotes the total flight time in μs, the y-axis the number of counted ions ($m/e = 32$). A shifted Maxwell–Boltzmann distribution convoluted over the finite chopper width is fitted to the data points and shown as a dotted line. The deviation between fit and data points is probably due to trapping of molecules in the QMS ionizer.

der Materie (FOM)', which is financially supported by the 'Nederlandse organisatie voor Wetenschappelijke Onderzoek (NWO)'.

References

[1] Raukema A, Dirksen R J and Kleyn A W 1995 *J. Chem. Phys.* **103** 6217
[2] Watts E and Sitz G O 1999 *J. Chem. Phys.* **111** 9791
[3] Murphy M J, Skelly J F, Hodgson A and Hammer B 1998 *J. Chem. Phys.* **109** 3619
[4] Rettner C T, DeLouise L A and Auerbach D J 1986 *J. Chem. Phys.* **85** 1131
[5] Hanisco T F, Yan C and Kummel A C 1992 *J. Chem. Phys.* **97** 1484
[6] Geuzebroek F H, Wiskerke M G, Tenner A E, Kleyn A W, Stolte S and Namike A 1991 *J. Phys. Chem.* **95** 8409
[7] Tenner M G, Geuzebroek F H, Kuipers E W, Wiskerke A E, Kleyn A W, Stolte S and Namike A 1990 *Chem. Phys. Lett.* **168** 45
[8] Huang Y H, Rettner C T, Auerbach D J and Wodtke A M 2000 *Science* **290** 111
[9] Hou H, Huang Y H, Gulding S J, Rettner C T, Auerbach D J and Wodtke A M 1999 *Science* **284** 1647
[10] Gostein M and Sitz G O 1997 *J. Chem. Phys.* **106** 7378
[11] McCabe P R, Juurlink L B F and Utz A L 2000 *Rev. Sci. Instrum.* **71** 42
[12] Juurlink L B F, Smith R L and Utz A L 2000 *J. Phys. Chem.* B **104** 3327
[13] Juurlink L B F, McCabe P R, Smith R L, DiCologero C L and Utz A L 1999 *Phys. Rev. Lett.* **83** 868
[14] Borroni-Bird C E and King D A 1991 *Rev. Sci. Instrum.* **62** 2177
[15] Holmblad P M, Wambach J and Chorkendorff I 1995 *J. Chem. Phys.* **102** 8255
[16] Romm L, Katz G, Kosloff R and Assher M 1997 *J. Phys. Chem.* B **101** 2213
[17] Wheeler M C, Seets D C and Mullins C B 1996 *J. Chem. Phys.* **105** 1572
[18] Hayden B E and Lamont C L A 1991 *Surf. Sci.* **243** 31
[19] Hayden B E and Godfrey D C 1990 *Surf. Sci.* **232** 24
[20] Oakes D J, Mc Coustra and Chesters M A 1993 *Faraday Discuss.* **96** 325
[21] Sullivan D J D and Kummel A C 1992 *Rev. Sci. Instrum.* **63** 4285
[22] Bonn M, Funk S, Hess Ch, Denzler D N, Stampfl C, Scheffler M, Wolf M and Ertl G 1999 *Science* **285** 1024
[23] Jenniskens H G, Bot A, Dorlandt P W F, van Essenberg W, de Haas E and Kleyn A W 1997 *Meas. Sci. Technol.* **8** 1313
[24] King D A and Wells M G 1972 *Surf. Sci.* **29** 454
[25] King D A and Wells M G 1974 *Proc. R. Soc.* **339** 245
[26] Raukema A 1995 Dynamics of chemisorption *PhD Thesis* University of Amsterdam
[27] Scoles G 1988 *Atomic and Molecular Beam Methods I* ed G Scoles (Oxford: Oxford University Press)